Theoretical Study of the Jahn−Teller Effect in $CH_3CN^+(\tilde{X}^2E)$ and $CD_3CN^+(\tilde{X}^2E)$: Multimode Spin-Vibronic Energy Level Calculations

Shiyang Zhang and Yuxiang Mo*

Department of Physics and Key Laboratory for Atomic and Molecular Nanosciences, Tsinghua University, Beijing 100084, China

Received: July 11, 2009; Revised Manuscript Received: August 21, 2009

The spin-vibronic energy levels for $CH_3CN^+(\tilde{X}^2E)$ and $CD_3CN^+(\tilde{X}^2E)$ have been calculated using a diabatic model including multimode vibronic couplings and spin−orbit interaction without adjusting any parameter. The diabatic potential energy surfaces are represented by the Taylor expansions including linear, quadratic and bilinear vibronic coupling terms. The normal coordinates used in the Taylor expansion were expressed by the mass-weighted Cartesian coordinates. The adiabatic potential energy surfaces for CH_3CN^+ and CD_3CN^+ were calculated at the level of CASPT2/cc-pvtz, and the spin−orbit coupling constant was calculated at the level of MRCI/CAS/cc-pvtz. The spin−orbit energy splittings for the ground vibrational states of $CH_3CN^+(\tilde{X}^2E)$ and $CD_3CN^+(\tilde{X}^2E)$ are 20 and 16 cm^{-1}, respectively, which are resulted from the quenching of the spin−orbit coupling strength of 51 cm^{-1}. The calculated spin-vibronic levels are in good agreement with the experimental data. The calculation results show that the Jahn−Teller effects in $CH_3CN^+(\tilde{X}^2E)$ and $CD_3CN^+(\tilde{X}^2E)$ are essential to understand their spin-vibronic energy structure.

I. Introduction

For two close-lying electronic states, a strong vibrational and electronic coupling between the two electronic states may occur, which result in vibrational energy levels that cannot be calculated using the Born−Oppenheimer approximation.[1] This is particularly true for degenerate electronic state due to symmetry of molecule, and the phenomenon is often called the Jahn−Teller (JT) effect for nonlinear molecule with C_{3v} or higher symmetries.[1−4] Recently, the vibronic energy levels for $CH_3O(\tilde{X}^2E)$, $CH_3S(\tilde{X}^2E)$,$CF_3O(\tilde{X}^2E)$, and $CF_3S(\tilde{X}^2E)$ molecules have been extensively studied using ab initio theoretical methods.[5−10] The calculation results usually reproduced the experimental data with accuracies around tens of wavenumbers. In the calculations, the nonadiabatic interactions are taken into consideration via diabatic Hamiltonian. In the diabatic Hamiltonian, the coupling between the nuclear vibrational motion and electronic motion is very small and can be neglected; however, the potential energy surfaces in the diabatic representation are subjected to "perturbation", or there are off-diagonal matrix elements in the diabatic potential energy matrix due to the lowering of the symmetry of the molecule.[1] The off-diagonal matrix elements can be determined via a number of methods. The most often used and also the simplest method is based on adiabatic energies calculated via various ab initio quantum chemistry methods. This formalism has been successfully applied to $CH_3O(\tilde{X}^2E)$, $CH_3S(\tilde{X}^2E)$, $CF_3O(\tilde{X}^2E)$, and $CF_3S(\tilde{X}^2E)$;[5−9] however, there are a few theoretical calculations performed for larger molecules with C_{3v} symmetry. The acetonitrile cation, $CH_3CN^+(\tilde{X}^2E)$, with degenerate electronic states provides an example of larger molecule with the Jahn−Teller effect.[11,12] Very recently, a theoretical study about the vibronic structure of CH_3CN^+ has been reported; however, it was mainly focused at the effect of vibronic interaction between the first electronically excited state and the ground state.[13] The theoretically calculated photoelectron spectra were compared with that measured experimentally with a resolution of ∼200 cm^{-1}, and no spin-vibronic energy levels have been provided.[11,13]

In 2005, we reported a high resolution zero-kinetic energy photoelectron (ZEKE) study of CH_3CN and CD_3CN with a spectral resolution of 2 cm^{-1}.[12] In the spectra, the lowest vibrational band of 235 cm^{-1} (196 cm^{-1}) for CH_3CN (CD_3CN) was found, which is much lower than the lowest vibrational band of 340 cm^{-1} (331 cm^{-1}) for neutral molecule and can be only explained by the presence of Jahn−Teller effect in the molecule. To assign the spectra, we used a single mode vibronic coupling model including linear and quadratic Jahn−Teller coupling to fit the experimental data, and the related spectroscopic parameters have been determined on the basis of this model.

To obtain further insights into the vibronic structure of $CH_3CN^+(\tilde{X}^2E)$, it is natural to ask if the previously used single mode coupling model can be based on a solid theoretical treatment, and if the vibronic energy levels can be calculated using ab initio method. In addition to this, a question was raised in the previous paper about the spin−orbit coupling in $CH_3CN^+(\tilde{X}^2E)$. From the bandwidths of the experimental data, it was guessed that the spin−orbit energy splitting for the vibrational ground state was around 10 cm^{-1}; however, the spin−orbit energy splitting constant was assumed to be zero in the fitting of the experimental data due to the limited resolution of the spectra. Since the spin−orbit coupling constant can be calculated with good accuracy for small molecules, a theoretical calculation of the spin−orbit coupling strength would provide us more insight into the experimental data and the relative importance between the Jahn−Teller effect and the spin−orbit coupling in the vibronic structure of $CH_3CN^+(\tilde{X}^2E)$.

In this work, we reported a calculation of vibronic energy levels for $CH_3CN^+(\tilde{X}^2E)$ and $CD_3CN^+(\tilde{X}^2E)$ using a diabatic model including multimode vibronic interaction and spin−orbit interaction without adjusting any parameter. The calculated spin-vibronic energy levels are in good agreement with experimental

* To whom correspondence should be addressed. E-mail: ymo@mail.tsinghua.edu.cn.

10.1021/jp906557n CCC: $40.75
Published on Web 09/17/2009

data. It is concluded that the Jahn−Teller effects are essential to understand the vibronic structure of $CH_3CN^+(\tilde{X}^2E)$ and$CD_3CN^+(\tilde{X}^2E)$.

II. Theoretical Model

The detailed description about the model Hamiltonian for spin-vibronic energy level calculation of C_{3v} symmetry molecules can be found in a number of publications.[1−10] Therefore, only a brief description will be given here. The diabatic model Hamiltonian H_{dia} is written as

$$H_{dia} = \begin{pmatrix} T_N + V_d + \frac{A_{SO}}{2}L_zS_z & V_{+,-} \\ V_{-,+} & T_N + V_d - \frac{A_{SO}}{2}L_zS_z \end{pmatrix} \quad (1)$$

where T_N is the kinetic energy operator for the nuclear vibration, L_zS_z represents the spin−obit interaction between the two splitting states, and A_{so} is the spin−orbit coupling constant. V_d and $V_{+,-}$ ($V_{-,+}$) are the diagonal and off-diagonal matrix elements for diabatic potential energy surfaces, respectively, and they can be calculated using the adiabatic energies for electronic states A′ and A″ formed by distorting the C_{3v} symmetry molecule with degenerate electronic state $\tilde{X}^2E$,

$$V_d = \frac{E(A') + E(A'')}{2} \quad (2a)$$

$$|V_{+,-}| = \frac{|E(A') - E(A'')|}{2} \quad (2b)$$

where E(A′) and E(A″) represent the adiabatic energies for A′ and A″ states of CH_3CN^+(X) (CD_3CN^+(X)), respectively. $|V_{+,-}|$ represents the modulus for the complex number. $|E(A')-E(A'')|$ represents the absolute value of $E(A')-E(A'')$.

For CH_3CN^+, there are four nondegenerate vibrational modes, e.g., symmetric C−H stretching (v_1), C≡N stretching (v_2), CH_3 umbrella (v_3), C−C stretching (v_4); and also four degenerate vibrational modes, e.g., asymmetric C−H stretching (v_5), CH_3 deformation (v_6), CH_3 rocking (v_7), and C−C≡N bending (v_8).

The Hamiltonian can be expressed by Taylor series using normal coordinates,[9]

$$V_d = \sum_{i=1}^{4}\frac{1}{2}\omega_i Q_i^2 + \sum_{j=5}^{8}\frac{1}{2}\omega_j Q_{j+}Q_{j-} + \frac{1}{6}\sum_{i=1,2} f_{iii}Q_i^3 + \frac{1}{24}\sum_{i=1,2} f_{iiii}Q_i^4 + \frac{1}{12}f_{555}(Q_{5+}{}^3 + Q_{5-}{}^3) + \frac{1}{2}f_{155}Q_1Q_{5+}Q_{5-} + \frac{1}{12}f_{1555}Q_1(Q_{5+}{}^3 + Q_{5-}{}^3) + \frac{1}{4}f_{1155}Q_1{}^2Q_{5+}Q_{5-} + \frac{1}{24}f_{5555}Q_{5+}{}^2Q_{5-}{}^2 \quad (3a)$$

$$V_{+,-} = \sum_{i=5}^{8} k_iQ_{i,-} + \sum_{i=5}^{8}\frac{1}{2}g_{i,i}Q_{i,+}^2 + \sum_{i=5,j=i+1}^{8} g_{i,j}Q_{i,+}Q_{j,+} + \sum_{i=1}^{4}\sum_{j=5}^{8} b_{i,j}Q_iQ_{j,-} \quad (3b)$$

$$V_{-,+} = V_{+,-}^* \quad (3c)$$

$$Q_{j\pm} = Q_{ja} \pm iQ_{jb} \quad (3d)$$

where ω_i is the harmonic frequency for ith vibrational mode, k_i is the linear JT parameter, g_{ii} and g_{ij} are the quadratic JT parameters for one mode or two-mode coupling, respectively, and $b_{i,j}$ is the bilinear JT parameter for the coupling between the symmetric and degenerate vibrational modes. Q_{ja} and Q_{jb} are the two Cartesian components for jth degenerate vibrational mode with A′ and A″ symmetries, respectively. In this work, we will mainly focus our attention at the vibronic energies not larger than 1200 cm^{-1}. It is found that the calculation results are not much affected by other higher order terms not listed in eqs 3a and 3b, which are hence neglected.

To solve the Hamiltonian matrix equation, we use the variation method. The basis set we used is

$$\Psi = |\Lambda S\Sigma\rangle\prod_{i=1}^{4}|v_i\rangle\prod_{j=5}^{8}|v_j,l_j\rangle \quad (4a)$$

$$l_j = -v_j, -v_j + 2, ..., v_j - 2, v_j \quad (4b)$$

where $\Lambda = +/-$ represents electronic state of A′/A″ symmetry, respectively. $S = {}^1/_2$ represents the electron spin, and $\Sigma = \pm{}^1/_2$ represents the projection of spin on the symmetric axis of the molecule. $|v_i\rangle$ represents the symmetric vibration of the ith mode, and $|v_j,l_j\rangle$ represents degenerate vibration of the jth mode with vibrational quantum number l_j.

III. Calculations for Potential Energy Surfaces (PESs) and Vibronic Parameters

The neutral CH_3CN and CD_3CN have C_{3v} geometrical structures, and the valence molecular orbitals for them can be represented as[11−13]

$$(4a_1)^2(5a_1)^2(6a_1)^2(1e)^4(7a_1)^2(2e)^4(3e)^0, X^1A'$$

where $7a_1$, 2e, and 3e orbitals correspond to chemical bonds of σ(C≡N), π(C≡N), and π^*(C≡N), respectively. The ground electronic state of the ion is formed by removing one electron out of the 2e orbital, and hence it has the symmetry of $\tilde{X}^2E$. However, when the nuclear vibrations deform the molecule to lower symmetry, C_s, the $\tilde{X}^2E$ state will be split into two states of $^2A'$ and $^2A''$ symmetries,

$$^2A', (...)(4a')^2(5a')^2(6a')^2(1a'')^2(7a')^2(8a')^2(2a'')^2(9a')^1$$

$$^2A'', (...)(4a')^2(5a')^2(6a')^2(1a'')^2(7a')^2(8a')^2(9a')^2(2a'')^1$$

To calculate the electronic energies at different geometric structures, we employed the complete active space second-order

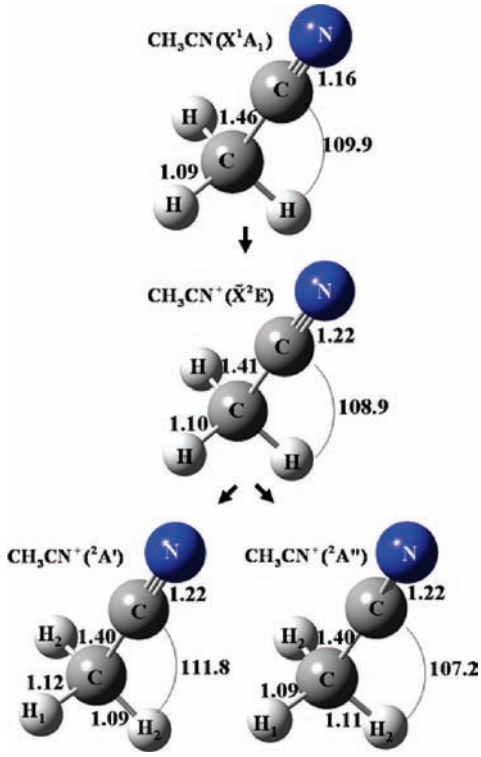

Figure 1. Minimum energy geometrical structures for $CH_3CN(\tilde{X}^1A')$, and $CH_3CN^+(\tilde{X}^2E)$ in C_{3v} and C_s symmetries, respectively. The optimization calculations were performed at the level of CASPT2/cc-pVTZ using the MOLPRO software.

TABLE 1: Calculated Geometrical Structures at the Minimum Energies for Neutral Molecule $CH_3CN(X^1A')$ and Cation $CH_3CN^+(\tilde{X})$ in C_{3v} and C_s Symmetries[a]

symmetry	r_{C-N}	r_{C-C}	r_{C-H_1}	r_{C-H_2}	α_{H_1CC}	α_{H_2CC}	$\alpha_{H_2CCH_1}$
X^1A_1[b]	1.16	1.46	1.09	1.09	109.9	109.9	120.0
X^1A_1[c]	1.17	1.46	1.09	1.09	109.2	109.2	120.0
$\tilde{X}^2E$[b]	1.22	1.41	1.09	1.09	108.9	108.9	120.0
$^2A'$[b]	1.22	1.40	1.12	1.09	102.8	111.8	114.3
$^2A''$[b]	1.22	1.40	1.09	1.11	112.7	107.2	124.7

[a] Bond lengths are in Å, and bond angles are in degree. [b] This work. The calculations were performed at the level of CASPT2/cc-pVTZ. The labels for atoms can be found in Figure 1. [c] From ref 13. The calculations were performed at the level of MP2/aug-cc-pVTZ.

perturbation method (CASPT2) with basis function cc-pVTZ. The active orbitals in C_s symmetry are (6a′)(1a″)(7a′)(8a′)(2a″)-(9a′)(3a″)(10a′) that corresponds to distribute 11 valence electrons into 8 orbitals, which can be represented by CAS(11,8).

The calculated minimum energy structures for neutral molecule $CH_3CN(\tilde{X}^1A')$, and cation $CH_3CN^+(\tilde{X}^2E)$ in C_{3v} symmetry, and C_s symmetry are shown in Figure 1, respectively. The optimizations were performed using the MOLPRO software package.[14] Table 1 shows the corresponding calculated geometric parameters along with the parameters of the neutral calculated at the level of MP2/aug-cc-pVTZ.[13] From Figure 1 and Table 1, it is clear that the geometrical changes resulting from the ionization are mainly in the bond lengths C≡N and C−C and bond angle H−C−C. The vibrational excitations related to these changes should be appear in the ZEKE spectra, which are just what is observed experimentally.[12] The minimum energy structure of $CH_3CN^+(\tilde{X}^2E)$ in C_{3v} symmetry is used as the reference point in the calculation of diabatic PES.

In the previous multimode vibronic calculations for C_{3v} molecules, the normal coordinates used in eq 3 are usually expressed by the symmetric internal coordinates.[5−9] This method is not easily generalized to larger molecules, for example for CH_3CN. In contrast with this, we used the mass-weighted Cartesian coordinates to represent the normal coordinates, which has been described by a number of textbooks.[15,16] It should be noted that in the present case the diabatic PESs (see eq 2) are used in determining the normal coordinates instead of the adiabatic PESs usually used. The second derivatives in the Hessian matrix were obtained by employing the numerical differentiation method with accuracy of second order relative to the nuclear displacements. The six normal coordinates corresponding to translational and rotational motions are separated from the vibrational modes in the molecular frame, which are done according to the well-established procedures.[15,16]

TABLE 2: Vibronic Parameters for the Diabatic Potential Energy Surface of $CH_3CN^+(\tilde{X})$[a]

CH_3CN^+: CASPT2/cc-pVTZ			
$\omega_1(A_1) = 2969$	$\omega_2(A_1) = 2030$	$\omega_3(A_1) = 1322$	$\omega_4(A_1) = 936$
$\omega_5(E) = 3070$	$\omega_6(E) = 1339$	$\omega_7(E) = 904$	$\omega_8(E) = 336$
$k_6 = -419$	$k_7 = -530$	$k_8 = 134$	$g_{66} = 21$
$g_{77} = -175$	$g_{88} = -69$	$g_{67} = 150$	$g_{68} = -26$
$g_{78} = 5$	$b_{26} = 0$	$b_{27} = 11$	$b_{28} = 8$
$b_{36} = -149$	$b_{37} = 31$	$b_{38} = -58$	$b_{46} = 56$
$b_{47} = 85$	$b_{48} = -13$		
$f_{111} = -960$	$f_{555} = 848$	$f_{155} = -1133$	$f_{1111} = 362$
$f_{5555} = 352$	$f_{1155} = 389$	$f_{1555} = -250$	$k_5 = 298$
$g_{55} = -21$	$b_{15} = 29$		
$f_{222} = 535$	$f_{2222} = 36$		
$A_{SO} = -51$			

[a] Units are in cm^{-1}. The parameters were obtained by the least-squares fittings using eqs 2 and 3. The coordinates Q in eq 3 are dimensionless. The adiabatic potential energies $E(A')$ and $E(A'')$ were calculated at the level of CASPT2/cc-pVTZ employing the MOLPRO software.[14] The coupling of v_1, v_2 and v_5 with other modes are neglected.

After obtaining the normal coordinates expressed by the mass-weighted Cartesian coordinates, we should calculate PESs representing by normal coordinates to obtain the vibronic parameters in eqs 2 and 3. Since the ab initio calculation software (MOLPRO) employs the Cartesian coordinates to determine the molecular geometry structure,[14] we have to transform the normal coordinates to the Cartesian coordinates. The points in normal coordinate space are sampled by the Monte Carlo method. In total, 700 geometric structures have been used to obtain PESs. The coefficients or vibronic parameters in the Taylor expression in eq 3 can be thus determined using the least-squares fitting method. To determine the vibronic parameters for the off-diagonal elements, we assume all the imaginary parts or Q_b are zero, and vary Q_a.[5−9] The calculated vibronic parameters are listed in Tables 2 and 3 for $CH_3CN^+(\tilde{X}^2E)$ and $CD_3CN^+(\tilde{X}^2E)$, respectively.

The spin−orbit coupling constant of $CH_3CN^+(\tilde{X}^2E)$ at the minimum energy geometrical structure in C_{3v} symmetry was calculated employing the MOLPRO software. Briefly, the calculation used the electronic wave function from multiconfiguration reference internally contracted configuration interaction (MRCI) method with the basis function of cc-pVTZ. The spin−orbit coupling matrix elements were calculated using the Breit−Pauli operator.[17] The calculated result is $A_{so} = -51\ cm^{-1}$. To test the accuracy at this level of calculation, we calculated the spin−orbit coupling constant of $HCN^+(\tilde{X}^2\Pi)$, which has been experimentally determined.[18] The result is $A_{so} = -51\ cm^{-1}$, which is similar to the experimentally determined spin−orbit energy splitting of $HCN^+(\tilde{X}^2\Pi)$ ($-49.8\ cm^{-1}$).[18] This indicates

TABLE 3: Vibronic Parameters for the Diabatic Potential Energy Surface of $CD_3CN^+(\tilde{X})$[a]

CD_3CN^+: CASPT2/cc-pVTZ			
$\omega_1(A_1) = 2127$	$\omega_2(A_1) = 2028$	$\omega_3(A_1) = 1073$	$\omega_4(A_1) = 836$
$\omega_5(E) = 2268$	$\omega_6(E) = 961$	$\omega_7(E) = 745$	$\omega_8(E) = 304$
$k_6 = -364$	$k_7 = -430$	$k_8 = 160$	$g_{66} = -12$
$g_{77} = 165$	$g_{88} = 65$	$g_{67} = -104$	$g_{68} = 21$
$g_{78} = -3$	$b_{26} = -1$	$b_{27} = -13$	$b_{28} = -2$
$b_{36} = 106$	$b_{37} = 1$	$b_{38} = 37$	$b_{46} = 7$
$b_{47} = -81$	$b_{48} = 55$		
$f_{111} = -547$	$f_{555} = 540$	$f_{155} = -707$	$f_{1111} = 115$
$f_{5555} = 443$	$f_{1155} = 162$	$f_{1555} = -136$	$k_5 = 299$
$g_{55} = -23$	$b_{15} = 25$		
$f_{222} = 536$	$f_{2222} = 161$		
$A_{SO} = -51$			

[a] Units are in cm^{-1}. The parameters were obtained by the least-squares fittings using eqs 2 and 3. The coordinates Q in eq 3 are dimensionless. The adiabatic potential energies $E(A')$ and $E(A'')$ were calculated at the level of CASPT2/cc-pVTZ employing the MOLPRO software.[14] The coupling of υ_1, υ_2 and υ_5 with other modes are neglected.

that the calculated spin−orbit coupling constant for $CH_3CN^+(\tilde{X}^2E)$ is a reliable value. The coincidence of the spin−orbit coupling constant of $CH_3CN^+(\tilde{X}^2E)$ with $HCN^+(\tilde{X}^2\Pi)$ is, in fact, not surprising because the spin−orbit coupling for these two molecules arise mainly from the π electrons located in the C≡N bonds.

Having determined the vibronic parameters and the spin−orbit coupling constant, the vibronic energy levels can be calculated using variational method with the basis function as shown in eq 4. The matrix elements can be calculated using the formula listed in the literature.[9] It is noted that the spin−orbit coupling constant is assumed to be independent of the geometrical structure of the molecule. The simultaneous calculation of all vibrational modes is out of our computation capability, we therefore only considered the couplings among the five vibrational modes (υ_3, υ_4, υ_6, υ_7, and υ_8). The coupling between them and the other three vibrational modes are weak for the energy region below 1400 cm^{-1} and were hence neglected. The maximum vibrational numbers used in the basis functions were 5, 5, 6, 8, and 10 for υ_3, υ_4, υ_6, υ_7, and υ_8, respectively. The full dimension of Hamiltonian for these basis functions is ~6×10^6. However, we have reduced the dimension to ~5.7×10^4 by excluding the basis functions with,

$$\sum_i \omega_i \upsilon_i > 8000\ \text{cm}^{-1} \text{ and } \sum_i |l_i| > 10$$

The eigenvalue equation was solved employing the Lancozs method. The eigenvalues lower than 1400 cm^{-1} for CH_3CN^+ or 1200 cm^{-1} for CD_3CN^+ are converged within 0.1 cm^{-1}.

For the calculation of spin-vibronic energies of υ_1 and υ_5, only the coupling between them has been considered. For the υ_2 vibrational mode, its coupling with other modes has been neglected. To take account of the quenching of spin−orbit coupling due to the Jahn−Teller effect arising from υ_6, υ_7, and υ_8 modes, effective spin−orbit constants of 20 and 16 cm^{-1} are assumed in these calculations, which are the first vibronic spin−orbit energy splittings of $CH_3CN^+(\tilde{X}^2E)$ and $CD_3CN^+(\tilde{X}^2E)$, respectively (see next section).

IV. Results and Discussion

(a) Overview. Table 4 shows the calculated spin-vibronic energy levels, their approximate assignments and the reported

TABLE 4: Ab Initio Calculated Vibronic Energy Levels for $CH_3CN^+(\tilde{X}^2E)$ and $CD_3CN^+(\tilde{X}^2E)$[a]

CH_3CN^+				CD_3CN^+			
assignment[b]		E_{cal}[c]	E_{exp}[d]	assignment[b]		E_{cal}[c]	E_{exp}[d]
$0_0(e)$	$e_{3/2}$	−10	0	$0_0(e)$	$e_{3/2}$	−8	0
$0_0(e)$	$e_{1/2}$	10	0	$0_0(e)$	$e_{1/2}$	8	0
$8_1(a_1)$	$e_{1/2}$	244	235	$8_1(a_1)$	$e_{1/2}$	198	196
$8_1(a_2)$	$e_{1/2}$	341		$8_1(a_2)$	$e_{1/2}$	299	
$8_1(e)$	$e_{1/2}$	351	360	$8_1(e)$	$e_{1/2}$	316	317
$8_1(e)$	$e_{3/2}$	356		$8_1(e)$	$e_{3/2}$	324	
$8_2(e)$	$e_{1/2}$	549	554	$8_2(e)$	$e_{1/2}$	469	
$8_2(e)$	$e_{3/2}$	556		$8_2(e)$	$e_{3/2}$	479	487
$7_1(a_1)$	$e_{1/2}$	603		$7_1(a_1)$	$e_{1/2}$	502	
$8_2(a_2)$	$e_{1/2}$	673		$8_2+7_1(a_2)$	$e_{1/2}$	599	
$8_2(a_1)$	$e_{1/2}$	686	683	$8_2+8_3(a_1)$	$e_{1/2}$	602	603
$8_2(e)$	$e_{3/2}$	691		$8_2+8_3(e)$	$e_{3/2}$	602	
$8_2(e)$	$e_{1/2}$	693		$8_2+8_3(e)$	$e_{1/2}$	605	
$7_1(a_2)$	$e_{1/2}$	809	804[e]	$7_18_1+7_1(e)$	$e_{1/2}$	709	
$8_3(e)$	$e_{3/2}$	856		$7_18_1+7_1(e)$	$e_{3/2}$	709	
$8_3(e)$	$e_{1/2}$	865		$7_1(a_2)$	$e_{1/2}$	711	680[e]
$8_3(a_1)$	$e_{1/2}$	869		$8_3(e)$	$e_{3/2}$	737	
$7_18_1(e)$	$e_{3/2}$	874		$8_3(e)$	$e_{1/2}$	747	
$7_18_1(e)$	$e_{1/2}$	878		$8_2(a_2)$	$e_{1/2}$	782	
$4_1(e)$	$e_{3/2}$	925	921[e]	$4_1(e)$	$e_{3/2}$	823	825
$4_1(e)$	$e_{1/2}$	941		$4_1(e)$	$e_{1/2}$	833	
$8_3(e)$	$e_{3/2}$	992		$8_3(e)$	$e_{3/2}$	868	
$8_3(e)$	$e_{1/2}$	1000		$8_3(e)$	$e_{1/2}$	868	
$8_3(e)$	$e_{1/2}$	1013		$4_1+8_3(e)$	$e_{3/2}$	871	
$8_3(e)$	$e_{3/2}$	1015		$4_1+4_18_3(e)$	$e_{1/2}$	875	
$8_3(a_2)$	$e_{1/2}$	1027		$6_1+7_18_1(e)$	$e_{1/2}$	886	
$7_1+7_2(e)$	$e_{1/2}$	1051		$7_1+6_1(e)$	$e_{3/2}$	891	
$7_1+7_2(e)$	$e_{3/2}$	1057		$8_3(a_2)$	$e_{1/2}$	892	
$7_18_1(e)$	$e_{1/2}$	1140		$6_1(a_1)$	$e_{1/2}$	905	
$7_18_1(e)$	$e_{3/2}$	1142		$6_1(a_2)$	$e_{1/2}$	950	943
$4_18_1+7_18_2(a_1)$	$e_{1/2}$	1145		$7_18_2+7_18_1(e)$	$e_{3/2}$	960	
$8_4(a_1)$	$e_{1/2}$	1161		$7_18_2+7_18_1(e)$	$e_{1/2}$	961	
$7_18_2(e)$	$e_{1/2}$	1179	1179[e]	$6_1+7_18_2(a_1)$	$e_{1/2}$	962	
$7_18_2(e)$	$e_{3/2}$	1180		$8_3+7_18_1(e)$	$e_{1/2}$	997[f]	
$8_4(a_2)$	$e_{1/2}$	1181		$8_3+8_2(e)$	$e_{3/2}$	997[f]	
$8_3+8_4(e)$	$e_{3/2}$	1187		$8_4+8_5(a_1)$	$e_{1/2}$	1001	
$8_3+8_4(e)$	$e_{1/2}$	1187		$8_4+8_5(a_2)$	$e_{1/2}$	1019	
$4_18_1(a_1)$	$e_{1/2}$	1191		$3_1(e)$	$e_{3/2}$	1026	
$4_18_1+6_1(a_2)$	$e_{1/2}$	1257		$3_1(e)$	$e_{1/2}$	1034	
$4_18_1(e)$	$e_{1/2}$	1271		$4_18_1(a_1)$	$e_{1/2}$	1045	
$3_1(e)$	$e_{3/2}$	1277		$8_3(e)$	$e_{3/2}$	1063	
$4_18_1(e)$	$e_{3/2}$	1284		$8_3(e)$	$e_{1/2}$	1065	
$6_1(a_1)$	$e_{1/2}$	1286		$3_1+6_1(e)$	$e_{3/2}$	1097	
$3_1(e)$	$e_{1/2}$	1293		$4_18_1(a_2)$	$e_{1/2}$	1103	
$6_1(a_2)$	$e_{1/2}$	1296		$3_1+6_1(e)$	$e_{1/2}$	1106	
$8_4(e)$	$e_{1/2}$	1307		$7_18_2+8_4(e)$	$e_{1/2}$	1125	
$8_4(e)$	$e_{3/2}$	1314		$7_18_2+6_18_1(e)$	$e_{3/2}$	1126	
$8_5(a_1)$	$e_{1/2}$	1323		$6_18_1(a_1)$	$e_{1/2}$	1136	
$8_4(e)$	$e_{1/2}$	1332		$8_4(a_1)$	$e_{1/2}$	1138	
$8_4(e)$	$e_{3/2}$	1342		$8_5(e)$	$e_{1/2}$	1140	
$8_4(e)$	$e_{1/2}$	1342		$6_18_1+8_1(e)$	$e_{3/2}$	1141[f]	
$7_18_1+7_28_1(e)$	$e_{3/2}$	1374		$8_4+8_5(e)$	$e_{3/2}$	1157[f]	
$7_18_1+7_28_1(e)$	$e_{1/2}$	1378		$8_4+8_5(e)$	$e_{1/2}$	1157[f]	
$2_1(e)$	e	2004	2004	$2_1(e)$	e	2020	2029
$5_1(a_1)$	$e_{1/2}$	2820		$1_1(e)$	$e_{3/2}$	2058	
$1_1(e)$	$e_{3/2}$	2856		$1_1(e)$	$e_{1/2}$	2071	
$1_1(e)$	$e_{1/2}$	2862		$5_1(a_1)$	$e_{1/2}$	2109	
$5_1(a_2)$	$e_{1/2}$	3027		$5_1(a_2)$	$e_{1/2}$	2284	
$5_1(e)$	$e_{1/2}$	3057		$5_1(e)$	$e_{1/2}$	2303	
$5_1(e)$	$e_{3/2}$	3062		$5_1(e)$	$e_{3/2}$	2314	

[a] Energy units are in cm^{-1}. [b] Assignments are only approximate. The rules for assignments are described in section IV(a). [c] This work. [d] From ref 12. [e] The assignment is different from the one given in ref. 12. [f] The state is highly mixed, and there is no vibronic state (see eq 4) with coefficient larger than 0.3 (probability 0.09). The two assignments are for spin-vibronic states with the two largest coefficients.

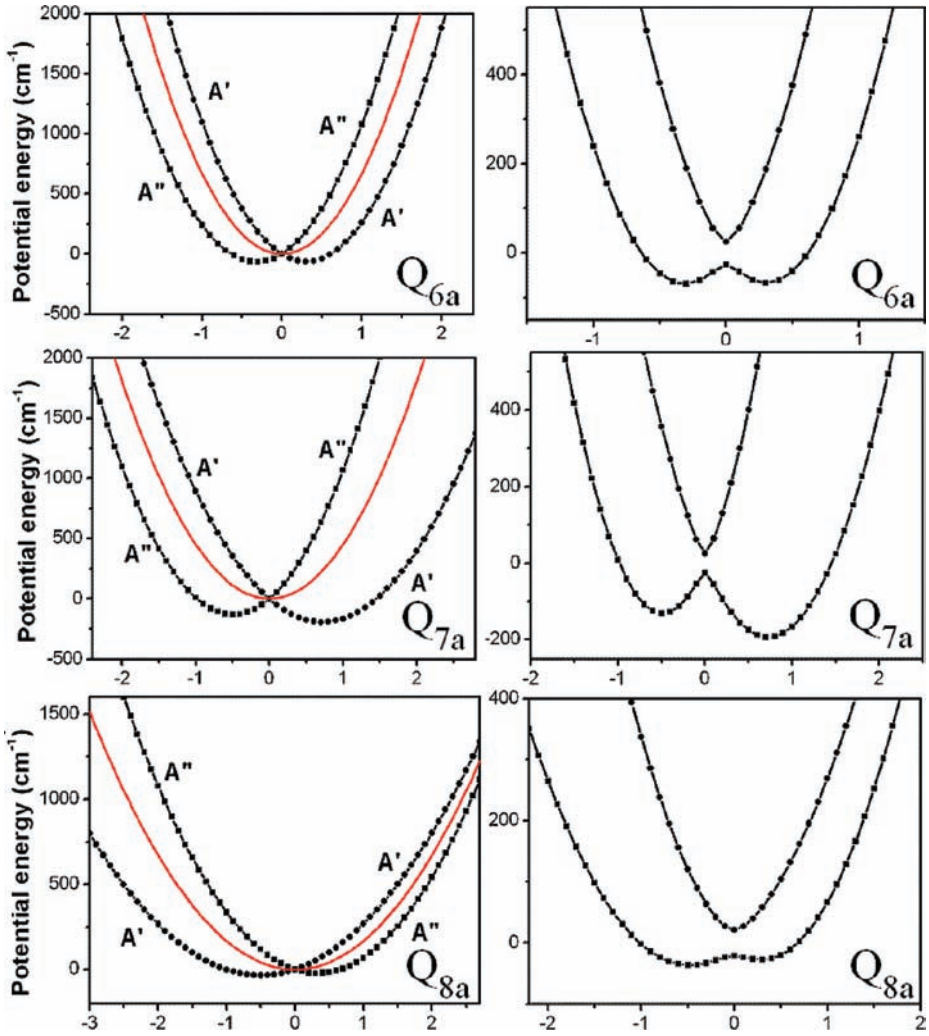

Figure 2. Slices of PESs for $CH_3CN^+(\tilde{X}^2E)$. Left column shows the slices of adiabatic PESs (in black color) and diabatic PESs (in red color) without accounting for the spin−orbit coupling. The diabatic PESs were calculated using $V_d = (E(A') + E(A''))/2$. Right column shows the slices of adiabatic PESs assuming spin−orbit coupling constant of 51 cm^{-1}. For both columns, from top to bottom *x*-coordinates are for normal coordinates Q_{6a}, Q_{7a}, and Q_{8a}, respectively, and all other normal coordinates were assumed to be zero in the calculations.

energy levels from the ZEKE experiments for $CH_3CN^+(\tilde{X})$ and $CD_3CN^+(\tilde{X})$.[12] Overall, the calculation results are in good agreement with the experimental data, especially for the first three spin-vibronic levels that are mainly due to the Jahn−Teller effect of C−C≡N bending vibration (υ_8). It is noted that the ZEKE spectra are not spin−orbit state resolved and the experimentally measured energy levels for the spin−orbit components $e_{1/2}$ and $e_{3/2}$ should be regarded as the average of two.

Since the vibrational frequency for the degenerate C−C≡N bending vibration (υ_8) is very small, the spin-vibronic state density is very high for state energy higher than 1000 cm^{-1}. As shown in Table 4, there are 10 spin-vibronic states for energies from 1293 to 1378 cm^{-1} for CH_3CN^+, and from 1103 to 1157 cm^{-1} for CD_3CN^+, respectively. Because each vibronic band has a rotational structure about 20−30 cm^{-1} for rotational temperature around 10 K, the vibronic bands in ZEKE spectra should be difficult to resolve just as those observed in experiments.[12] This is one of the reasons that we have not extended the calculation to higher energy states for vibrational modes of υ_3, υ_4, υ_6, υ_7, and υ_8.

Because there are strong vibronic mixings and also multimode mixings, the assignments for energy levels based on the basis functions are only approximate. We have set up the following rules to guide the assignments: (1) if the coefficient (absolute value) for a basis function is larger than 0.5 (probability 0.25), then the assignment is the state with the largest coefficient; (2) if there is no state with coefficient (absolute value) larger than 0.5, then all states with coefficients larger than 0.3 (probability 0.09) are written down. However, if there is only one state with coefficient (absolute value) larger than 0.3, then the term with the second largest coefficient will also be written down; (3) if there is no state with coefficient (absolute value) larger than 0.3, two states with the largest coefficients are written down, and a superscript "f" is labeled to the corresponding energy level in Table 4.

(b) Potential Energy Surfaces (PESs) and Spin−Orbit Splitting. Figure 2 shows the slices of 3-D PES of $CH_3CN^+(\tilde{X}^2E)$ for normal coordinates of Q_{6a}, Q_{7a}, and Q_{8a}, respectively, all other normal coordinates are assumed to be zero. As mentioned earlier, Q_{ia} components have A′ symmetries. For the left column of Figure 2, the black curves are the slices from the adiabatic PES without accounting for the spin−orbit coupling, and the red ones represent the slices from the diabatic PES calculated using eq 2a. The right column of Figure 2 shows the slices of adiabatic PES with spin−orbit coupling constant of 51 cm^{-1}. Figure 3 shows a glimpse view of 3-D PES for υ_8 vibrational mode of $CH_3CN^+(\tilde{X}^2E)$.

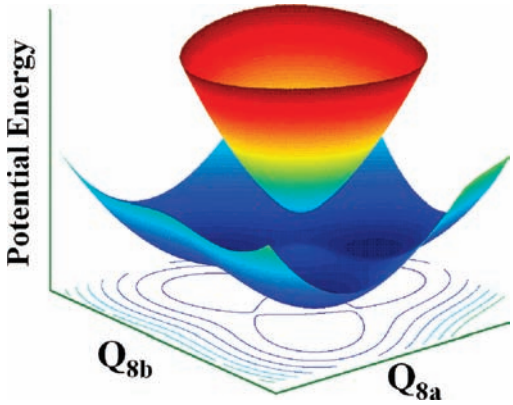

Figure 3. Adiabatic PES of $CH_3CN^+(\tilde{X}^2E)$ for υ_8 vibrational mode including spin−orbit interaction. A cut of PES can be found in the right column of Figure 2.

TABLE 5: Jahn−Teller Stabilization Energies (E_{JT}) and Barriers to Pseudo-Rotation (Δ_{JT}) for Individual Vibrational Modes and for Potential Energy Surfaces[a]

	E_{JT}		Δ_{JT}	
mode	CH_3CN^+	CD_3CN^+	CH_3CN^+	CD_3CN^+
υ_5	14	19	1	1
υ_6	60	65	−2	−3
υ_7	185	153	62	53
υ_8	32	49	11	16
sum[b]	291	286	72	67
PES[c]	283	283	47	47

[a] Units are in cm^{-1}. E_{JT} is the energy difference between the lowest adiabatic energy at C_s geometry and the minimum energy at C_{3v} geometry. Δ_{JT} is the energy difference between the two minimum energies at C_{2v} geometry with A″ and A′ symmetries. E_{JT} and Δ_{JT} for the first four rows are determined for each vibrational modes, respectively. [b] Summations for four degenerate vibrations. [c] E_{JT} and Δ_{JT} obtained from the PES including all coordinates. Because of the multimode interactions, their values are different from the summation values of different vibrational modes.

In Figure 2, $Q_{ja} = 0$ ($j = 6$, 7, and 8) indicates that the geometry of the molecule is at C_{3v} symmetry, and other values of Q_{ja} indicate that the geometry of the molecule is at C_s symmetry. It is clear that the deformation of geometric structure from C_{3v} to C_s will lower the energies or the Jahn−Teller effect, as shown in Figure 2. Two parameters are often used to qualitatively characterize the Jahn−Teller effect, the Jahn−Teller stabilization energy (E_{JT}) and barrier to pseudorotation or the quadratic Jahn−Teller stabilization energy (Δ_{JT}).[3−9] E_{JT} is the potential energy difference between the lowest adiabatic energies at C_s and C_{3v} geometry structures. Δ_{JT} is the potential energy difference between the two minimum energies at C_s geometry structures with A′ and A″ symmetries. Table 5 lists the values of E_{JT} and Δ_{JT} for υ_5 υ_6, υ_7, and υ_8 vibrational modes, respectively.

From Table 5, it is known that the E_{JT} and Δ_{JT} for each vibrational mode are different, and the vibrational mode υ_7 has the largest E_{JT} and Δ_{JT} among the four degenerate vibrational modes. Summations of E_{JT} and Δ_{JT} for all vibrational modes are also listed in Table 5. However, the summations are usually different from E_{JT} and Δ_{JT} determined directly from the PESs considering all coordinates. The reason for this is that the geometric positions for the minimum energies in the PES are different from the combined geometric positions for the minimum energies of all vibrational modes when there are multimode interactions. The E_{JT} and Δ_{JT} directly from the PESs

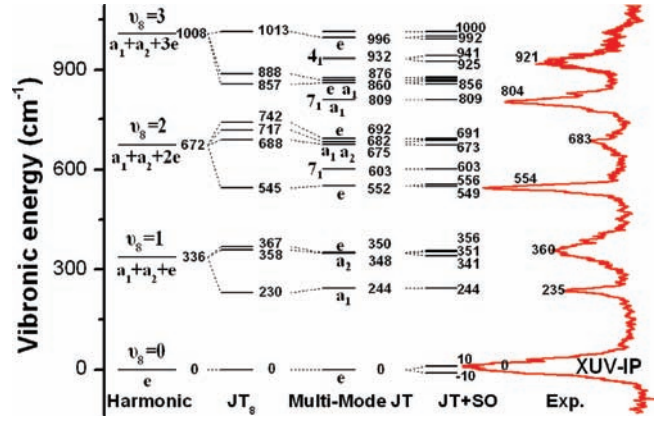

Figure 4. Ab initio calculated vibronic energy levels and the experimental observations for $CH_3CN^+(\tilde{X}^2E)$. The column "Harmonic" shows the harmonic energy levels. The column "JT_8" shows the vibronic energy levels from single mode approximation. The column "Multi-Mode JT" shows the vibronic energy levels accounting for the multimode interactions. The column "JT+SO" shows the vibronic energy levels accounting for both the multimode and the spin−orbit interactions. The column "Exp." shows the experimental spectra from ref 12.

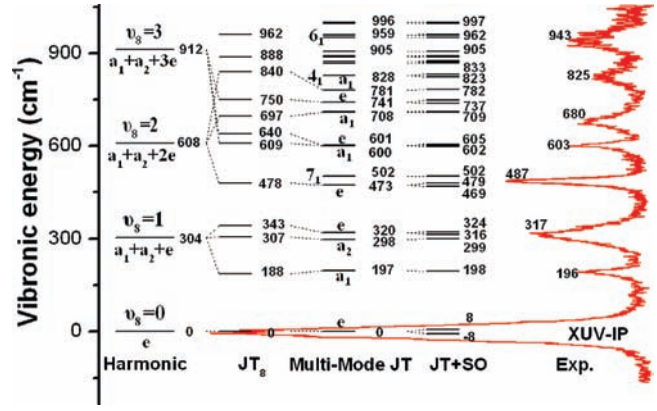

Figure 5. Ab initio calculated vibronic energy levels and the experimental observations for $CD_3CN^+(\tilde{X}^2E)$. The column "Harmonic" shows the harmonic energy levels. The column "JT_8" shows the vibronic energy levels from single mode approximation. The column "Multi-Mode JT" shows the vibronic energy levels accounting for the multimode interactions. The column "JT+SO" shows the vibronic energy levels accounting for both the multimode and the spin−orbit interactions. The column "Exp." shows the experimental spectra from ref 12.

are also listed in Table 5. The summation of E_{JT} is more than 5 times larger than the spin−orbit coupling strength (51 cm^{-1}). It is therefore expected that the Jahn−Teller effect is the major factor in determining the vibronic structure of $CH_3CN^+(\tilde{X}^2E)$ and $CD_3CN^+(\tilde{X}^2E)$; however, the spin−orbit interactions in them are not small enough to be neglected in the vibronic energy level calculations.

(c) Jahn−Teller Active Vibrational Modes. There are four Jahn−Teller active modes (υ_5−υ_8) or asymmetric C−H stretching vibration (υ_5), CH_3 deformation (υ_6), CH_3 rock (υ_7), and C−C≡N bending vibration (υ_8). Among the four modes, υ_8 has the lowest fundamental vibrational energy levels, and many related vibrational excitations have been observed in the experimental ZEKE spectra.[12]

Figures 4 and 5 show the multimode vibronic coupling effect in the calculation of energy levels for $CH_3CN^+(\tilde{X}^2E)$ and $CD_3CN^+(\tilde{X}^2E)$, respectively. The ZEKE spectra from ref 12 are also shown in the figures for comparison. It is seen that the

TABLE 6: Comparison of Experimentally Determined and Theoretically Calculated Jahn-Teller Parameters for $CH_3CN^+(\tilde{X}^2E)$ and $CD_3CN^+(\tilde{X}^2E)$[a]

	ω_8	k_8	g_{88}
	$CH_3CN^+(\tilde{X}^2E)$		
experimental[b]	329	147	43[c]
theoretical[d]	336	134	−69
	$CD_3CN^+(\tilde{X}^2E)$		
experimental[b]	302	135	66
theoretical[d]	304	160	65

[a] Units are cm^{-1}. [b] Experimentally determined parameters from ref 12, which were obtained by fitting the observed energy levels assuming υ_8 the only Jahn−Teller active mode. The original parameters have been transformed to the present definition (see eq 3). [c] The experimental value is positive. However, the experimental fittings could only determine the absolution value of the parameter when using single mode approximation. [d] Theoretically calculated parameters from this work.

first three lowest energy levels are from the splittings of the fundamental C−C≡N bending vibration. As shown in Figures 4 and 5, the single mode calculations provide a good description of the first four excited vibronic bands of υ_8 for both $CH_3CN^+(\tilde{X}^2E)$ and $CD_3CN^+(\tilde{X}^2E)$, and not much improvement has been obtained by accounting for the multimode couplings, which justifies the data fitting method used in the previous publication.[12] The reason is that the C−C≡N bending vibration frequency is much lower than other vibrational modes, and the first four excited vibronic bands have been not much affected by the multimode couplings. However, the spin−orbit energy splittings do provide insight into the experimental spectra. For example, the first and third vibrational bands (0 and 360 cm^{-1} for CH_3CN^+, 0 and 317 cm^{-1} for CD_3CN^+, respectively) are apparently broader than the second bands (235 cm^{-1} for CH_3CN^+, and 196 cm^{-1} for CD_3CN^+),[12] which arise from the fact that there are spin−orbit splittings for the first and third vibrational bands, and no spin−orbit splitting for the second bands. It is also noted that for higher excitations of υ_8 its couplings with other modes, in particularly with υ_7, are strong.

Table 6 shows the JT parameters determined from ZEKE spectra and also the calculated parameters. The JT parameters from the experiments have been obtained by assuming υ_8 to be the only Jahn−Teller active mode and fitting the experimental data.[12] It is seen that the agreement between the experimentally determined parameters and the calculated parameters are quite good, which provides another evidence indicating the weak coupling of υ_8 with other vibrational modes in low excitation energy region.

The first vibrational state of CH_3 deformation (υ_7) for CH_3CN^+ splits into four energy levels due to the vibronic interaction: 603 (a_1), 809 (a_2), 1051 ($e_{1/2}$), and 1057 ($e_{3/2}$) cm^{-1}. In the ZEKE spectra of CH_3CN^+, there is a vibrational band at 804 cm^{-1} that was assigned as the fundamental vibrational band of C−C stretching (υ_4).[12] With the present calculation result, the band at 804 cm^{-1} should be assigned as the band of υ_7 or $7(a_2)$, as shown in Table 4.

For CD_3CN^+, the first vibrational state of υ_7 splits into two levels of 502 (a_1) and 711 (a_2) cm^{-1} that can be assigned unambiguously. The spin−orbit components $e_{3/2}$ and $e_{1/2}$ for it are difficult to find due to the strong mode mixing between υ_7 and υ_8. The band at 680 cm^{-1} in the ZEKE spectra was originally assigned from the Jahn−Teller excitation of $3\upsilon_8$.[12] On the basis of the present calculations, this band should be assigned as $7_1(a_2)$.

TABLE 7: Calculated Spin−Orbit Energy (SO) Splittings for the First Vibrational Energy Levels and Ground Vibronic State (IP)[a]

	υ_1[b]	υ_2[c]	υ_3	υ_4	υ_5[b]	υ_6[d]	υ_7	υ_8	IP
CH_3CN^+	6	20	16	16	−5		−6	−5	20
CD_3CN^+	13	16	8	10	−11		*d*	−8	16

[a] Units are cm^{-1}. For degenerate vibrations υ_5 to υ_8, the first vibrational states split into four levels with symmetries a_1, a_2, $e_{1/2}$, and $e_{3/2}$. The SO splittings are the energy difference between the spin−orbit components of $e_{1/2}$ and $e_{3/2}$. [b] In the calculation, only the coupling between υ_1 and υ_5 has been considered, and effective spin−orbit coupling constants of 20 and 16 cm^{-1} were assumed to account for the Jahn−Teller effect due to other modes for CH_3CN^+ and CD_3CN^+, respectively. [c] The coupling of υ_2 with other vibrational modes is neglected, the SO splitting should be therefore the same as that of the ground vibrational state. [d] The assignments are difficult because of strong mixing among different spin vibronic states; see section IV(a) and (c) for details.

The strong mixings between υ_7 and υ_8 for CD_3CN^+ are not resulted from direct coupling of two modes, as the coupling coefficient, $g_{78} = -3$ cm^{-1}, is very small. The strong mixings arise from indirect couplings via the ground vibronic state, as pointed out by Barckholtz and Miller.[2] For the first several υ_8 excitation bands, the assignments are unambiguous. For higher excitation, it is found that the assignment to a particular vibrational number and even to a particular mode is difficult. For an example, the leading terms of the wave function corresponding to the energy level 886 cm^{-1} is

$$0.23|-\rangle|8_2,0\rangle - 0.28|-\rangle|8_1,1\rangle|7_1,-1\rangle - 0.23|+\rangle|8_2,2\rangle + 0.24|+\rangle|8_4,2\rangle - 0.26|+\rangle|7_1,-1\rangle - 0.31|+\rangle|6_1,-1\rangle + \ldots \quad (5)$$

where $|+\rangle$ and $|-\rangle$ represent $\Lambda = 1$ or -1, respectively. Σ is fixed to $^1/_2$ (see eq 4 for definition of the basis function). It is noted that the values of the coefficients for different basis functions in eq 5 are not much different, showing strong mixing among these basis states. This state is assigned as $6_1+7_18_1(e_{1/2})$ according to our rules for assignments (see section IV(a)).

The first vibrational state of CH_3 deformation (υ_6) for CH_3CN^+ splits into two levels of 1286 (a_1) and 1296 (a_2) cm^{-1}. The spin−orbit components $e_{1/2}$ and $e_{3/2}$ for it have not been found due to the strong mixings among vibronic modes. However, it is certain that fundamentals of υ_6 fall in the broad peak region of the ZEKE spectrum and have not been observed experimentally.[12] The band at 1179 cm^{-1} in the ZEKE paper was assigned as the fundamental band of υ_6,[12] which is wrong on the basis of the present calculation. The band at 1179 cm^{-1} may be tentatively assigned as combinational band of $7_18_2(e)$. For CD_3CN^+, the fundamental vibrational band of υ_6 splits into two levels 905 (a_1) and 950 (a_2) cm^{-1}. The spin-obit components $e_{3/2}$ and $e_{1/2}$ for it cannot been determined. The band at 943 cm^{-1} in the ZEKE spectra was assigned as 6_1.[12] With the present calculation, this band should be more reasonably assigned as $6_1(a_2)$ band.

The first vibrational state of asymmetric C−H and C−D stretching (υ_5) are 2820 and 2109 cm^{-1} for CH_3CN^+ and CD_3CN^+, respectively, which lie in the very broad peak region of the ZEKE spectra and have not been identified experimentally.[12]

To see the interaction between the vibronic coupling and spin−orbit coupling, Table 7 lists the spin−orbit energy splittings for the first vibronic states of all vibrational modes.

It is seen that the spin−orbit energy splittings are further reduced for the first excited vibronic states in comparison with the vibronic ground states.

(d). First Excited Vibronic Energy levels for Symmetric Vibrational Modes. The symmetric vibrational modes include C−H stretching (υ_1), C≡N stretching (υ_2), CH_3 umbrella vibration (υ_3), and C−C stretching (υ_4) vibrations. In the ZEKE spectra,[12] the C≡N stretching (υ_2) is the most active among the symmetric vibrational modes since the bond length C≡N is increased from 1.16 to 1.22 Å upon ionization. As we mentioned in section III, in the calculation of the υ_2 vibrational mode its coupling with other modes has been neglected, and the calculation aims to provide theoretical fundamental vibrational energy levels for υ_2, which are in good agreement with the experimental data as shown in the bottom of Table 4.

The fundamental vibrational band for C−C stretching (υ_4) in the ZEKE spectra of CD_3CN^+ was assigned as a band at 825 cm^{-1}.[12] The corresponding calculated energy levels are 823 and 833 cm^{-1} for spin−orbit components $e_{1/2}$ and $e_{3/2}$, respectively, which are in good agreement with the experimental data. As mentioned above, in the ZEKE paper the assignment for υ_4 fundamental band of CH_3CN^+ is wrong. On the basis of the present calculation, the band at 921 cm^{-1} assigned as $(JT)^9$ in the ZEKE spectra should be assigned as fundamental bands of υ_4 whose calculated values are 925 and 941 cm^{-1} for spin−orbit components $e_{3/2}$ and $e_{1/2}$, respectively.[12]

The fundamental bands of υ_1 and υ_3 for CH_3CN^+ and CD_3CN^+ all fall in the broad peak region of the ZEKE spectra, and have not been observed experimentally.[12] The calculation values for both vibrational modes can be found in Table 4.

It is noted that due to the bilinear interactions between the symmetric vibrational modes and the degenerate vibrational modes the spin−orbit energy splittings for the first vibrational state of symmetric modes are usually smaller than the values at the ground vibronic state, as shown in Table 7. If there is no bilinear interaction, the spin−orbit energy splittings for symmetric modes should be similar to that in the ground vibronic state of the molecule.[6]

V. Summary

The spin-vibronic energy levels for $CH_3CN^+(\tilde{X}^2E)$ and $CD_3CN^+(\tilde{X}^2E)$ have been calculated using a diabatic model including multimode vibronic coupling and spin−orbit interaction.[5−9] The adiabatic PESs for CH_3CN^+ and CD_3CN^+ were calculated at the level of CASPT2/cc-pvtz. The spin−orbit coupling constant was calculated at the level of MRCI/CAS/cc-pvtz. The diabatic PESs are represented by the Taylor expansions including linear, quadratic and bilinear vibronic coupling terms for vibrational modes of symmetric CH_3 (CD_3) umbrella vibration (υ_3), symmetric C−C stretching (υ_4), degenerate CH_3 (CD_3) deformation (υ_6), degenerate CH_3 (CD_3) rocking (υ_7), and degenerate C−C≡N bending (υ_8). The vibronic energy levels for symmetric C−H stretching (υ_1) and asymmetric C−H stretching vibrations (υ_5) have been calculated considering only the interaction among themselves. For the calculation for C≡N stretching vibration (υ_2), the couplings with other modes are all neglected. The calculated spin-vibronic energy levels are in good agreement with the experimental data.

It is found that spin−orbit energy splittings of the ground vibronic states for $CH_3CN^+(\tilde{X}^2E)$ and $CD_3CN^+(\tilde{X}^2E)$ are 20 and 16 cm^{-1}, respectively, which are resulted from the quenching of the spin−orbit coupling strength, 51 cm^{-1}. The bilinear couplings between the symmetric and degenerate vibrations result in further reduction of spin−orbit energy splittings for the first vibrational energy levels of the symmetric vibration modes, which was pointed out previously for CH_3O.[6]

On the basis of the present calculations, three important assignments about the previous ZEKE spectra have been revised.[12] The fundamental band of C−C stretching vibration (υ_4) for $CH_3CN^+(\tilde{X}^2E)$ is assigned as band at 921 cm^{-1}, while the previously assigned υ_4 band at 804 cm^{-1} is assigned as $7_1(a_2)$ band. For $CD_3CN^+(\tilde{X}^2E)$, the fundamental CH_3 rocking (υ_7) vibrational band was assigned as a band at 680 cm^{-1}.

Acknowledgment. We are grateful to Dr. A. V. Marenich and Prof. J. E. Boggs in University of Texas at Austin, and Prof. H. Köppel in University of Heidelberg, Germany, for their kindness to answer our questions about the calculation methods. This work is funded by Projects 20673066, 20773076, and 10734040 supported by the National Science Foundation of China, and Project 2007CB815200 supported by NKBRSF of China.

References and Notes

(1) *Conical Intersections: Electronic Structure, Dynamics & Spectroscopy*; Domcke, W., Yarkony, D. R., Kǫppel, H., Eds.; World Scientific: River Edge, NJ, 2004.
(2) Barckholtz, T. A.; Miller, T. A. *Int. Rev. Phys. Chem.* **1998**, *17*, 435.
(3) Applegate, B. E.; Barckholtz, T. A.; Miller, T. A. *Chem. Soc. Rev.* **2003**, *32*, 3.
(4) Paterson, M. J.; Bearpark, M. J.; Robb, M. A.; Blancafort, L.; Worth, G. A. *Phys. Chem. Chem. Phys.* **2005**, *7*, 2100.
(5) Hoper, U.; Botschwina, P.; Köppel, H. *J. Chem. Phys.* **2000**, *112*, 4132.
(6) Schmidt-Kluegmann, J.; Köppel, H.; Schmatz, S.; Botschwina, P. *Chem. Phys. Lett.* **2003**, 369–21.
(7) Marenich, A. V.; Boggs, J. E. *J. Phys. Chem. A* **2004**, *108*, 10594.
(8) Marenich, A. V.; Boggs, J. E. *J. Chem. Phys.* **2005**, *122*, 024308.
(9) Marenich, A. V.; Boggs, J. E. *J. Phys. Chem. A* **2007**, *111*, 11220.
(10) Schuurman, M. S.; Weinberg, D. E.; Yarkony, D. R. *J. Chem. Phys.* **2007**, *127*, 104309.
(11) Gochel-Dupuis, M.; Delwiche, J.; Hubin-Franskin, M. J.; Collin, J. E. *Chem. Phys. Lett.* **1992**, *193*, 41.
(12) Yang, J.; Zhou, C.; Mo, Y. *J. Phys. Chem. A* **2005**, *109*, 9964.
(13) Ghanta, S.; Mahapatra, S. *Chem. Phys.* **2008**, *347*, 97.
(14) MOLPRO, version 2006.1, a package of ab initio programs; Werner, H. J., Knowles, P. J., Lindh, R., Manby, F. R., Schutz, M. See: http://www.molpro.net.
(15) Wilson, E. B.; Decius, J. C.; Cross P. C. *Molecular Vibrations*; McGraw-Hill: New York, 1955.
(16) Bunker, P. R., Jensen, P. *Molecular symmetry and spectroscopy*, 2nd ed.; NRC Research Press: Ottawa, 1998.
(17) Berning, A.; Schweizer, M.; Werner, H. J.; Knowles, P. J.; Palmieri, P. *Mol. Phys.* **2000**, *98*, 1823.
(18) Wiedmann, R.; White, M. G. *J. Chem. Phys.* **1995**, *102*, 5141.

JP906557N